



Research Article

White Light-Emitting Diode Coated with $K_3Lu(PO_4)_2$: Tb^{3+} , Eu^{3+} Nanocrystal Films Enveloped by SiO_2

Nguyen Van Dung¹, Nguyen Huy Khiem², Phan Xuan Le^{2,*}

¹Faculty of Engineering, Dong Nai Technology University, Bien Hoa City, 76000, Vietnam

²Faculty of Electrical Engineering Technology, Industrial University of Ho Chi Minh City, Ho Chi Minh City, 70000, Vietnam

*Corresponding author: phanxuanle@iuh.edu.vn; Tel.: +840986959404

Abstract: A series of novel adjustable-illumination including $K_3Lu(PO_4)_2$: Tb^{3+} , and Eu^{3+} (KLPO:Tb,Eu) phosphors with improved energy-transfer efficiency were made using strong-heat solid-state (SS) reactivity. X-ray diffractivity (XRD), luminescence spectroscopy, chromatic coordination, and fluorescence decomposition analyses were used to describe the materials. The first-principles method during the analysis was used to investigate power band structure as well as denseness for statuses in $K_3Lu(PO_4)_2$. The result showed that the doping dose ratio for Tb^{3+}/Eu^{3+} was found to be the main factor controlling the energy transmission (ET) between Tb^{3+} and Eu^{3+} elements. The ET between Tb-Eu was governed by an electric dipole-dipole interaction which produced tunable emissions from green to orange-red regions. During the study, a 365 nm chip was incorporated with BaMgAl10O17: Eu^{2+} blue phosphor, SiAlON: Eu^{2+} green phosphor, and $K_3Lu(PO_4)_2$:0.1 Tb^{3+} ,0.06 Eu^{3+} (KLPO:0.1Tb,0.06Eu) orange-red phosphor to create a triple-phosphor-based white light-emitting diode (WLED). The device generated white light featuring a great chroma rendition indicator reaching 91.4 as well as an acceptable associated chroma temperature reaching 3678 K. These properties showed that the developing phosphor was suitable for warm WLED applications, as the performance was comparable to those of perfect white light.

Keywords: Eu^{3+} ; Multi-color tuning; Power transition; SiO_2 ; Tb^{3+} ; Warm WLED

1. Introduction

White light-emitting diode units (WLEDs) are semiconductors that may become transformed into phosphorus and have several exceptional qualities, including high energy converting effectiveness, color tunability, long lifespan, small size, environmental friendliness, as well as dependability (Tung et al., 2024). These qualities enable the devices to effectively replace traditional incandescent and fluorescent lamps. Following the discussion, LED has two different types of parts. The first is near-ultraviolet (UV) or blue LED chip, where other consists of phosphors made of rare-earth replacement substances (Anh et al., 2024). The total light-emitting effectiveness, color rendition, and heat stability of the resulting white illumination are therefore all determined by phosphor, allowing it to be a crucial element (Tung et al., 2024). Up until recently, adding $Y_3Al_5O_{12}:Ce^{3+}$ (YAG:Ce) to cover LED chips in blue was the easiest and most popular way to form commercial WLED (Anh et al., 2024; Le et al., 2024). The white illumination generated by this device has color flaws in green and red zones, detrimentally impeding practicality as well as leads to a poor color rendering intent lower than 80 as well as elevated correlated color temperature (CCT) greater than 4500 K (Tung et al., 2024). Increasing the proportion of red emissions is necessary to improve the efficiency of WLED (Huu and

This work was supported by the National Kaohsiung University of Science and Technology, for providing software and experiment support

<https://doi.org/10.14716/ijtech.v16i3.6022>

Received October 2022; Revised April 2023; Accepted May 2023

Thi, 2022). Additionally, the supply of phosphors in the market has an inadequate red bandwidth, which dramatically lowers CCT and color rendering intent (CRI). The development of the red luminescent phosphor suitable to be coupled for making LED with outstanding CRI and acceptable CCT is an extensively investigated topic in this direction. Under such states, there is a necessity for examining three-color illuminating phosphor samples proficiently roused by near-UV radioactivity and satisfy the specifications of white illumination industrial LED devices (My et al., 2022).

Rare-earth (RE) ions are crucial in current screen lighting, photodetection, optic amplification, and further relevant applications due to the exceptional luminous qualities as well as distinct emitting bands (Le et al., 2022). Based on common knowledge, illumination of centric RE elements results from the proficient ET between the trinity status for ligand and the crystalline field statuses (Tran et al., 2020). Therefore, ET has a significant impact on both theory and practice when it comes to the color tuning of phosphors (Tran et al., 2020). Relating to the discussion, Tb³⁺ element would be the activator with highest utilization frequency within phosphor samples. Based on the dopant amount, the emission results from ⁵D₃→⁷F_j transition within blue zones or ⁵D₄→⁷F_j mechanism (J = 6–2) within green zones (Thai et al., 2023). The interactivity among Tb³⁺ element shows greater potency under surging Tb³⁺ presence, leading to a cross-alleviation amid ⁵D₃ as well as ⁵D₄ levels and the induction of ⁵D₄→⁷F_j shift featuring primarily green radioactivity (Zhang et al., 2022; Lui, et al., 2019). Moreover, the red component in disparate Tb³⁺ and Eu³⁺ joint-integrated phosphor samples can be compensated for by magnetism dual-polar shift between ⁵D₀ and ⁷F₁ as well as electrical dual-polar shift between ⁵D₀ and ⁷F₂ in Eu³⁺ element, respectively (Mohamed et al., 2020). The interactivity from phosphate categories (PO₄)³⁻ in orthophosphate variants comprising functioning elements, including Eu³⁺ as well as Tb³⁺, leads to extremely high power-converting effectiveness in addition to effective UV photon energy absorption (Wang et al., 2017). This qualifies phosphate as the main component in near-UV white-illumination LED.

According to this study, a novel high-temperature solid-state KLPO:Tb,Eu phosphor with controllable illumination emission was created. The latticework configuration as well as electron characteristics for the base KLPO were modeled using Density functional theory (DFT) method in Vienna Ab-initio simulation Package (VASP) program because of the dearth of data on the luminous properties of KLPO phosphors. In addition, several analytical methods, including luminescence spectroscopy, X-ray diffractivity (XRD), and photoelectron spectroscopic assessment (XPS) were used for clarifying the luminous characteristics of the KLPO:Tb,Eu. The outcomes showed the promise of KLPO:Tb,Eu for UV WLED color tunability.

2. Experimental

2.1. Substances and combination

K₃Lu_{1-x-y}(PO₄)₂ series: xTb³⁺, yEu³⁺ Phosphors were formed using traditional high-temperature solid-state process (x = 0, 0.07-0.13; y = 0-0.26). The raw ingredients were stoichiometric high-purity, including Lu₂O₃ (99.99%), NH₄H₂PO₄ (99%), Tb₄O₇ (99.99%), and Eu₂O₃ (99.99%), which made it possible to prevent future cleansing before use. During the process, the granules were well combined and afterward mixed in an agate mortar. Mixtures were then heated again for 4 hours at 800 °C, and sintered in a muffle for 4 hours at 1150 °C. The finished specimens were crushed into fine powders after being cooled to room temperature for further characterization (Kumar and Nishchal, 2019).

2.2. Manufacturing a model of LED

The commercial SiAlON:Eu²⁺ green powder and BaMgAl₁₀O₁₇: Eu²⁺ blue powder BAM were combined with KLPO:0.1Tb,0.06Eu orange powder in a proportion of 10: 1: 2. The powdered compound was mixed unto UV chip (1 W, ex = 365 nm) as well as OE6550 silica gel as a fixing agent to create a WLED. Figure 1 showed the technical details of WLED during the process.

2.3. Characterization

At room temperature, XRD was used to analyze the phase element and clarity of numerous typical powder specimens. The X-ray diffractivity profile was obtained in the range of 5° ≤ 2θ ≤

80° applying a diffractometric apparatus operating at a voltage of up to 40 kilovolts and a current reaching 30 milliamperes, using one Cu K α pipe in form of luminous means ($\lambda = 0.15406$ nm) (Thi et al., 2023a). During the process, the Rietveld rectification was conducted via GSAS program. The chemical composition as well as elemental valent property were ascertained via XPS utilizing one ESCALAB Xi+ electron spectrometer. The fluorescence spectrophotometer PL system Hitachi F-4700 was used to collect the luminescence stimulation/emission (PLE/PL) spectra, and the system was fitted with a 400 V, 150 W Xe lamp. Additionally, a spectrofluorometer with a 150 W xenon illumination supply was used to calculate the quantum yield (Thi et al., 2023b). An FS5 spectrofluorometer fitted via one 150-W CW ozoneless Xe arc light captured the normal-temperature fluorescence decay curves (Reyes-Alberto et al., 2023; Gong et al., 2021).

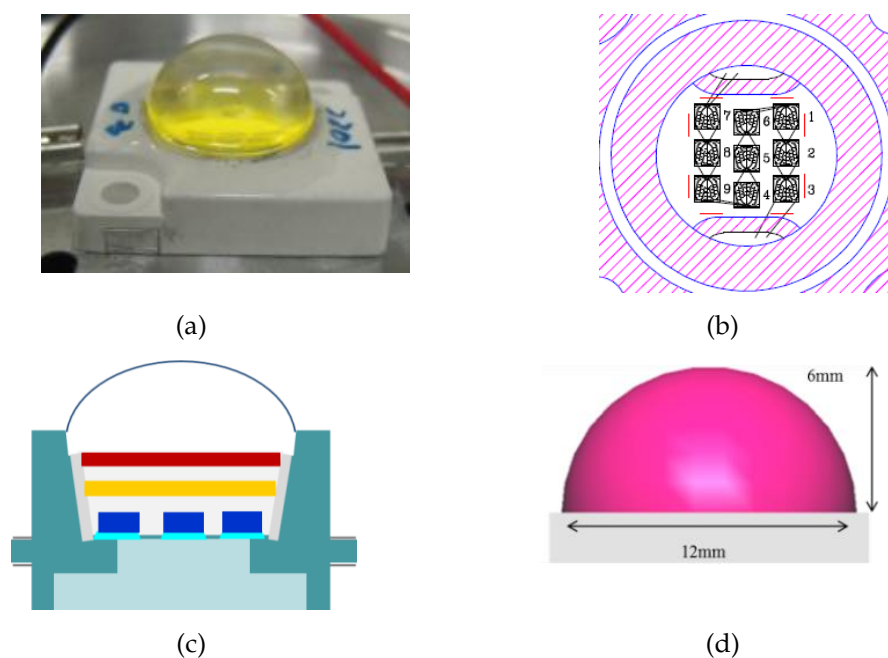


Figure 1 Picture showing utilized WLED: (a) WLED used in the research herein, (b) Tethering setting, (c) Graphic depiction for WLED, (d) WLED recreation using LightTools program

The analysis created spherical, almost mono-disperse silica particles using Stober method (Wang and Sun, 2020). In previous studies, water and TEOS were used as a couple of the reactants, methanol or ethanol as the solvent, and ammonium hydroxide as the catalyst to produce silica nanoparticles with diameters ranging from 10 to 450 nm (Mohan and Negi, 2024; Shaban et al., 2020; Chan et al., 2010). As the dosages for TEOS as well as NH₄OH decreased and that of water increased, the particle size declined. Nearly monodispersed silica nanoparticles with diameters ranging from 50 to 450 nm could be generated as ethanol was employed in the form of the solvating agent. Consequently, when methanol was used, silica nanoparticles with dimensions ranging from 10 to 50 nm could be produced. Due to variations in nucleus size generated in each solvent, the particle size varied depending on the solvent used. Virtually monodispersing and globular nanogranules were formed when particles exceeded 25 nm in diameter. On the other hand, main silica nanoparticle aggregates with a network topology smaller than 25 nm developed. The reaction temperature and method were adjusted, as shown in Figure 2, to lessen the size of the silica nanoparticles as well as prevent aggregate formation. Figures 2(a)-(e) corresponds to disparate silica nanoparticle sizes, including 5%, 10%, 15%, 20%, and 25%, respectively.

3. Results and Discussion

The power gap was estimated using Kubelka-Munk function to further distinguish when KLPO was an indirect or direct band gap substance.

$$[F(R_{\infty})/hv]^n = C(hv - E_g) \quad (1)$$

Where hv was the photoenergy, R_{∞} represented reflectivity, and E_g signified optic band gap power. The combination was considered one straightforward band gap agent with n equal to 2. Following the discussion, the non-direct band gap was signified via $n = 1/2$.

The emitting color was adjusted from Tb^{3+} -integrated samples using an effective CR procedure among identical Tb^{3+} ions in extra to ET among various Tb^{3+} as well as Eu^{3+} ionic granules. The procedure used for Tb^{3+} during the analysis was explained as follows (Yu et al., 2021).

$${}^5D_3(Tb_{3+}) + {}^7F_6(Tb_{3+}) - {}^5D_4(Tb_{3+}) + {}^7F_0(Tb_{3+}) \quad (2)$$

The process was performed since the energy gaps between 5D_3 - 5D_4 (5725 cm^{-1}) and 7F_6 - 7F_0 (6000 cm^{-1}) stated were comparable. When the positions of Tb^{3+} ionic granules were close enough, a resonance ET was probably to occur, in which the transfer of electrons from 7F_6 - 7F_0 was followed by the relaxation of electrons from 5D_3 to 5D_4 (Zhou et al., 2021).

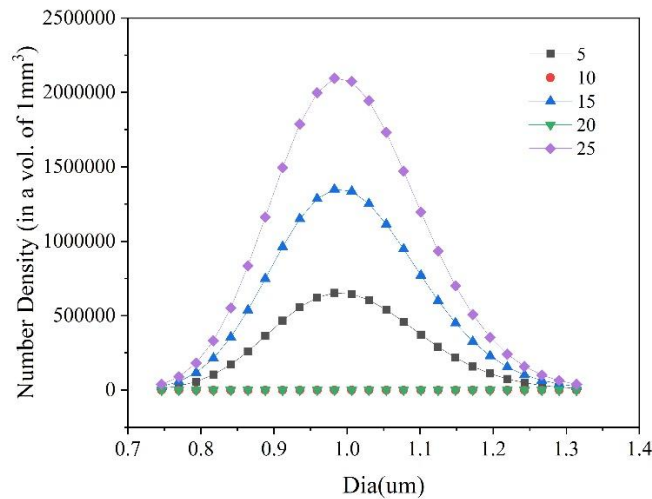


Figure 2 Number density of $K_3Lu(PO_4)_2:Tb^{3+}, Eu^{3+}$ phosphor particles: 5%-25%

Based on the process, a dual-exponential decay function matched the deterioration arch well (Huang et al., 2019):

$$I(t) = A_1 \exp(-t/\tau_1) + A_2 \exp(-t/\tau_2) \quad (3)$$

Where $I(t)$ represented the Tb^{3+} emitting strengths at the delay period of t , τ_1 and τ_2 were the exponential component's quick and slow fluorescence durations, and t signified the delay period. Additionally, A_1 and A_2 represented the particular constant values. Calculations for the mean duration (τ^*) were as follows (Francois et al., 2021):

$$\tau^* = (A_1\tau_1^2 + A_2\tau_2^2) / (A_1\tau_1 + A_2\tau_2) \quad (4)$$

Figure 3 showed YGA:Ce phosphor dose based on SiO_2 particle sizes. When SiO_2 particle size was 25 wt.%, YGA:Ce dosage hit the lowest point at 24.5%. Consequently, YGA:Ce dosage reached the highest points at 27.5 - 28.5% when the particle sizes were approximately 5 wt.%. During the process, YGA:Ce dosage increased when the particle sizes were reduced. Figure 4 showed the color variations (CCT) depending on SiO_2 particle sizes. CCT value reached the peak at over 3150 K when the particle size was 5 μm and achieved the lowest point at ~ 2950 K when the particle size was 15 μm . Moreover, CCT value stayed quite steadily at ~ 3000 K with particle sizes of 25 μm . The value would be greatest with the appropriate particle sizes of 5 μm .

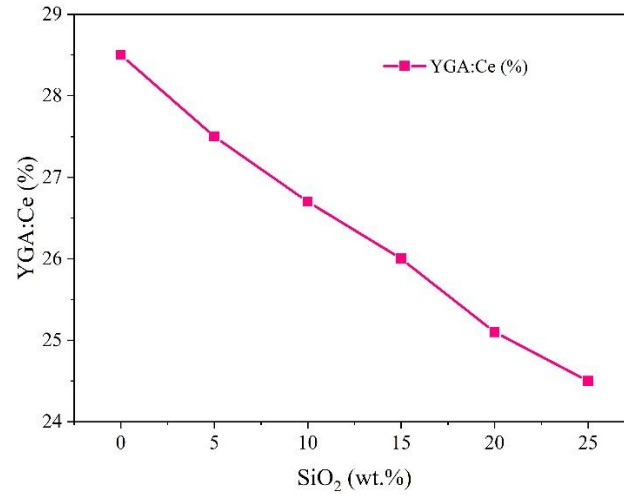


Figure 3 The dosage of YGA:Ce phosphor according to SiO₂ concentration

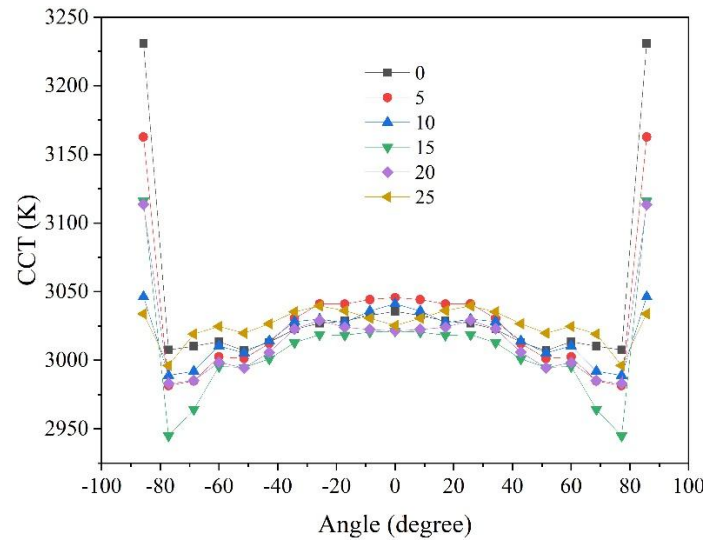


Figure 4 CCT variations according to SiO₂ concentration

Equation (3) and (4) were used to find the precise values of A_1 , A_2 , τ_1 , τ_2 , and the mean decay period. When Eu^{3+} content increased, the emitting lifespan of Tb^{3+} reduced monotonically, supporting the existence of an active additional decomposition channel and ET of phosphor from Tb^{3+} to Eu^{3+} . In Tb/Eu ET procedure, the transmission probability ($P_{\text{Tb-Eu}}$) was represented as follows (Liu et al., 2020).

$$P_{\text{Tb-Eu}} = (1/\tau_x) - (1/\tau_0) \quad (5)$$

Where τ_x and τ_0 were the lives of Tb^{3+} both being presented and not of Eu^{3+} for the equal sensitizer doses, accordingly. The process showed a plot of the computed degradation periods and $P_{\text{Tb-Eu}}$ values against Eu^{3+} doses. Moreover, the following formula was used to compute the power transition effectiveness (η_T) from Tb^{3+} to Eu^{3+} ions (Bui et al., 2020).

$$\eta_T = 1 - (\tau_x / \tau_0) \quad (6)$$

Where τ_x signified the lifespan for Tb^{3+} within the joint-doped Tb, Eu samples, τ_0 was the radioactive deterioration lifespan for Tb^{3+} , while η_T was the energy transition efficient. The transference performance increased from 26.93% towards nearly 100% as Eu presence surged, which surpassed the bulk of Tb/Eu co-doped value of phosphors.

Figure 5 showed color deviation variations (D-CCT) according to SiO₂ particle sizes. D-CCT values reached the peaks at 180–220 K when the particle sizes were up to 5 wt.%. The value hit the

smallest point at 40 K when the particle size was 25 wt.%. Accordingly, D-CCT value was greatest with the suitable particle sizes at ~5 wt.%. Figure 6 showed the light-emitting beam by LED during the analysis. When the particle sizes were 0 – 10 wt.%, there were maximum lumen values at nearly 73.5. On the other hand, lumen value was around 71 when the particle size was 15 wt.%. The particle sizes 0 – 10 wt.% were the greatest for lumen output during the process.

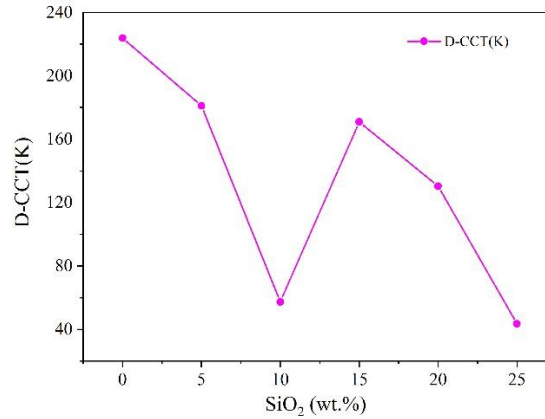


Figure 5 Investigation of the color deviation changes according to SiO₂ concentration

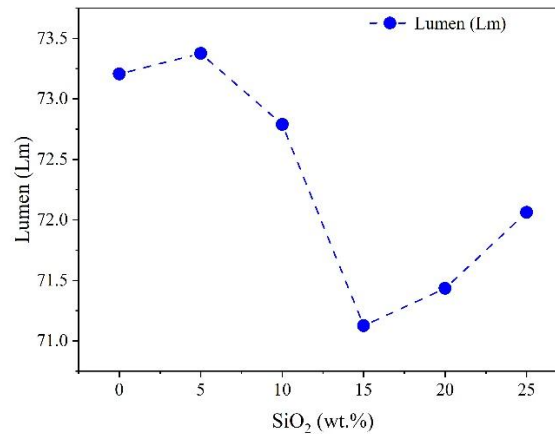


Figure 6 The luminous flux emitted by LED according to the concentration change of SiO₂

Blasse estimated that the crucial separation R_c for ET from Tb³⁺ to Eu³⁺ was as follows (Toslak et al., 2020).

$$R_c \approx 2[3V / 4\pi x_c N]^{\frac{1}{3}} \quad (7)$$

Where x_c was the combined dosage of Tb³⁺ and Eu³⁺, N signified the quantity for formulaic elements within a unit cellule, V represented the volume for said cellule. Consequently, since the associated R_c reached 10.274 Å, well surpassing 5 Å, the multipolar interactivity led to ET activity.

The multipole interaction governed the resonance power transition from Tb³⁺ to Eu³⁺ in KLPO:Tb,Eu phosphors. Reisfeld's theory and Dexter's formula allowed the study to examine ET process using the following equation (Yang et al., 2019).

$$\eta_0 / \eta \approx I_{so} / I_s \alpha C^{n/3} \quad (8)$$

I_s as well as I_{so} were the illumination strengths for Tb³⁺ having and not having Eu³⁺. In line with this process, C represented Eu³⁺-doping concentration, and n was the interaction types. When n equaled 6, 8, and 10, the interactions were assigned to dipole-dipole, dipole-quadrupole, as well as quadrupole-quadrupole types, respectively. Following this analysis, η_0 and η were the light-emitting quantum effectiveness (QEs).

The emitting strengths of Tb^{3+} and Eu^{3+} were lessened via heat abatement to 68.1% and 84.0% of those at room temperature. During the process, Arrhenius expression was employed for determining activation energy (ΔE) as well as examining the heating consistency (Beldi et al., 2019; Feng et al., 2019).

$$\ln(I_0 / I_T) = \ln A - \Delta E / kT \quad (9)$$

Where I_0 and I_T were, luminous intensity of KLPO:0.1Tb,0.06Eu phosphor at normal heat as well as a specific heat.

Figure 7 showed the changes of CRI as well as CQS values, respectively. Both CRI and CQS values tended to decrease as the particle sizes increased. CRI value decreased from approximately 56.2 to 55.7 when the particle sizes increased from 0 to 25 wt.%. Similarly, CQS value reduced from about 42.5 to 39.5 as the particle sizes increased from 0 to 25 wt.%. Figure 8 showed the emission spectra of WLED during the analysis. At various phosphor concentrations, a visible emission range with a maximum point around 600 nm was observed. The outcome signified that the luminescence at this wavelength in WLED could improve color properties of the device, including color rendering index (CRI), variation of the angular CCT, and color quality scale (CQS).

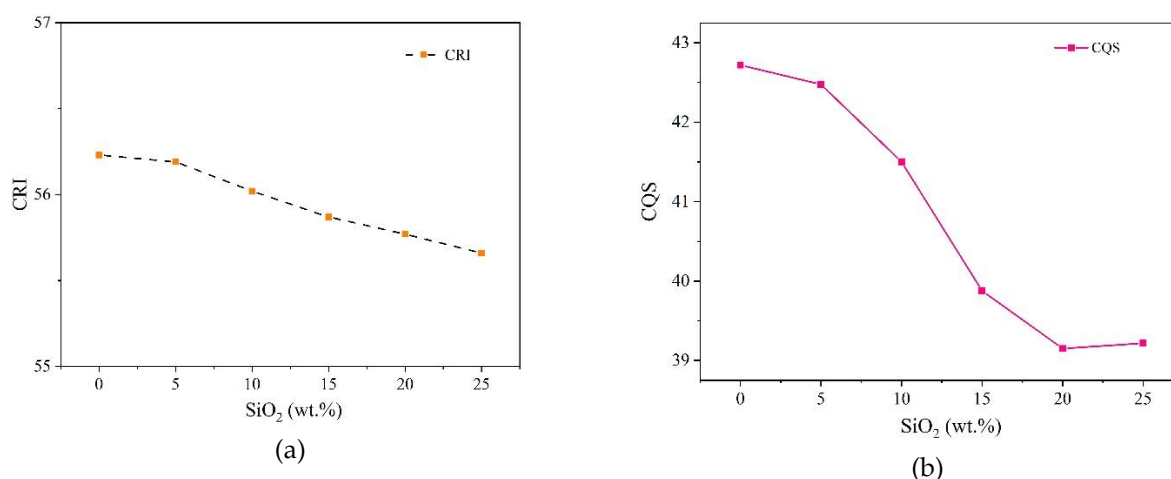


Figure 7 CRI (a) and CQS (b) variations according to SiO₂ concentration

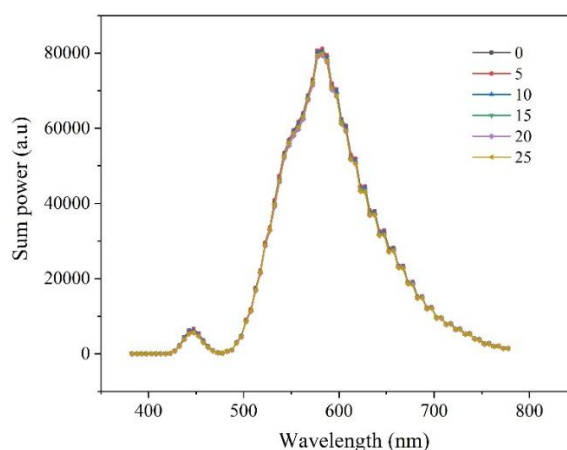


Figure 8 Spectrum color range according to SiO₂ concentration

4. Conclusions

In conclusion, a sequence of $K_3Lu(PO_4)_2:xTb^{3+},yEu^{3+}$ phosphors with a sole composition and color-adjustable radiation were made via the strong-heat SS reactivity. KLPO host passed through crystallization in a trilateral setting featuring P-3 (147) spatial category, as confirmed by Rietveld

refinement data. This host was identified as a direct bandgap substance based on the band structure analysis of KLPO. The band obtained via the structural graph (5.3537 eV) highly resembled its counterpart acquired via the dispersal reflection arch (5.59 eV). Relating to the discussion, luminescence investigations showed that Tb³⁺ could proficiently sensitize the emission for Eu³⁺ subject to UV stimulation. The associated ET became subject to regulation via the dipole-dipole process during the analysis. Furthermore, increasing Eu³⁺ composition allowed ET effectiveness to reach a value of up to 98.36%. As a result, the discharge chroma for KLPO:Tb,Eu samples, ranging between yellow-green and orange-red could be tuned by adjusting Tb/Eu dosage ratio. Finally, the white illumination generated by white LED using near-UV LED apparatuses presented great CRIs (Ra = 91.4) and a suitable CCT when applying KLPO:0.1Tb,0.06Eu phosphor (3678 K). These results showed that KLPO:Tb,Eu was a promising phosphor component for near-UV LED applications.

Acknowledgements

The authors would like to thank Professor Hsiao-Yi Lee, National Kaohsiung University of Science and Technology, for providing software and experiment support.

Author Contributions

Nguyen Van Dung (nguyenvandung@dntu.edu.vn): Software, Validation, Investigation, Resources, Data Curation, Review, Visualization.

Nguyen Huy Khiem: Conceptualization, Methodology, Software, Validation, Investigation, Resources, Data Curation, Writing, Review, Editing, Visualization

Phan Xuan Le: Conceptualization, Methodology, Software, Validation, Investigation, Resources, Data Curation, Writing, Review, Editing, Visualization, Supervision, Project administration

Conflict of Interest

The authors declare no conflicts of interest.

References

Anh, NDQ & Lee, HY 2024, 'Titanium dioxide in vanadate red phosphor compound for conventional white light emitting diodes', *Optoelectronics and Advanced Materials - Rapid Communications*, vol. 18, pp. 480-484

Anh, NDQ 2024, 'Nano scattering particle: an approach to improve quality of the commercial led', *The University of Danang - Journal of Science and Technology*, pp. 53-57, <https://doi.org/10.31130/ud-jst.2024.614e>

Beldi, S, Boussaha, F, Hu, J, Monfardini, A, Traini, A, Bertrand, FL, Chaumont, C, Gonzales, M, Firminy, J, Reix, F, Rosticher, M, Mignot, S, Piat, M & Bonifacio, P 2019, 'High Q-factor near infrared and visible Al₂O₃-based parallel-plate capacitor kinetic inductance detectors', *Opt. Express*, vol. 27, pp. 13319-13328, <https://doi.org/10.1364/OE.27.013319>

Bui, HQT, Velpula, RT, Jian, B, Philip, MR, Tong, HD, Lenka, TR & Nguyen, HPT 2020, 'High-performance nanowire ultraviolet light-emitting diodes with potassium hydroxide and ammonium sulfide surface passivation', *Appl. Opt.*, vol. 59, pp. 7352-7356, <https://doi.org/10.1364/AO.400877>

Chan, QN, Medwell, PR, Kalt, PaM, Alwahabi, ZT, Dally, BB & Nathan, GJ 2010, 'Solvent effects on two-line atomic fluorescence of indium', *Applied Optics*, vol. 49, no. 8, pp. 1257-1266, <https://doi.org/10.1364/AO.49.001257>

Feng, S & Wu, J 2019, 'Color lensless in-line holographic microscope with sunlight illumination for weakly-scattered amplitude objects', *OSA Continuum*, vol. 2, pp. 9-16, <https://doi.org/10.1364/OSAC.2.000009>

Francois, EL, Herrnsdorf, J, McKendry, JJD, Broadbent, L, Wright, G, Dawson, MD & Strain, MJ 2021, 'Synchronization-free top-down illumination photometric stereo imaging using light-emitting diodes and a mobile device', *Opt. Express*, vol. 29, pp. 1502-1515, <https://doi.org/10.1364/OE.408658>

Gong, S, Wu, R, Yang, S, Wu, L, Zhang, M, Han, Q & Wu, W 2021, 'Tuning the luminous properties and optical thermometry of Cs₂SnCl₆ phosphor microcrystals via Bi and Sb codoping', *Photon. Res.*, vol. 9, pp. 2182-2189, <https://doi.org/10.1364/PRJ.431672>

Huang, C, Chang, Y, Han, L, Chen, F, Li, S & Hong, J 2019, 'Bandwidth correction of spectral measurement based on Levenberg–Marquardt algorithm with improved Tikhonov regularization', *Appl. Opt.*, vol. 58, pp. 2166-2173, <https://doi.org/10.1364/AO.58.002166>

Huu, PD & Thi, DAN 2022, 'Selection of multi-layer remote phosphor structure for heightened chromaticity and luminous performance of white light-emitting diodes', *International Journal of Technology*, vol. 13, no. 4, pp. 837-847, <https://doi.org/10.14716/ijtech.v13i4.5051>

Kumar, P & Nishchal, NK 2019, 'Enhanced exclusive-OR and quick response code-based image encryption through incoherent illumination', *Appl. Opt.*, vol. 58, pp. 1408-1412, <https://doi.org/10.1364/AO.58.001408>

Le, PX, Anh, NDQ & Lee, HY 2024, 'Regulating the white LED properties with different SiO₂ particle sizes', *Optoelectronics and Advanced Materials - Rapid Communications*, vol. 18, pp.485-489

Le, PX, Trang, TT, Anh, NDQ, Lee, H-Y & Tho, LV 2022, 'Comparison between SEPs of CaCO₃ and TiO₂ in phosphor layer for better color uniformity and stable luminous flux of WLEDs with 7,000 K', *Materials Science Poland*, vol. 40, pp. 1–8, <https://doi.org/10.2478/msp-2022-0008>

Liu, Q, Liu, Y, Pointer, MR, Huang, Z, Wu, X, Chen, Z & Luo, MR 2020, 'Color discrimination metric based on the neutrality of lighting and color transposition quantification', *Opt. Lett.*, vol. 45, pp. 6062-6065, <https://doi.org/10.1364/OL.400422>

Lui, J, Vegni, AM, Colace, L, Neri, A & Menon, C 2019, 'Preliminary design and characterization of a low-cost and low-power visible light positioning system', *Appl. Opt.*, vol. 58, pp. 7181-7188, <https://doi.org/10.1364/AO.58.007181>

Mohamed, HEA, Hkiri, K, Khenfouch, M, Dhlamini, S, Henini, M & Maaza, M 2020, 'Optical properties of biosynthesized nanoscaled Eu₂O₃ for red luminescence applications', *Journal of the Optical Society of America A*, vol. 37, no. 11, pp. C73-C79, <https://doi.org/10.1364/JOSAA.396244>

Mohan, S, & Negi, M 2024, 'SiO₂-capped ZnO quantum dots based highly sensitive optical fiber humidity sensor with potential applications in human breath monitoring and voice print recognition', *Applied Optics*, vol. 63, no. 30, pp. 7955-7963, <https://doi.org/10.1364/AO.533760>

My, LTT, Thai, NL, Bui, TM, Lee, H-Y & Anh, NDQ 2022, 'Phosphor conversion for WLEDs: YBO₃:Ce³⁺,Tb³⁺ and its effects on the luminous intensity and chromatic properties of dual-layer WLED model', *Materials Science Poland*, vol. 40, pp. 105–113, <https://doi.org/10.2478/msp-2022-0050>

Reyes-Alberto, M, García-Valenzuela, A & Gutierrez-Herrera, E 2023, 'Method for measuring the extinction coefficient of fluorescing media within the emission band', *Applied Optics*, vol. 62, no. 8, pp. C106-C114, <https://doi.org/10.1364/AO.478433>

Shaban, SM, Mehaney, A, & Aly, AH 2020, 'Determination of 1-propanol, ethanol, and methanol concentrations in water based on a one-dimensional phoxonic crystal sensor,' *Applied Optics*, vol. 59, no. 13, pp. 3878-3885, <https://doi.org/10.1364/AO.388763>

Shi, Y, Ye, S, Yu, J, Liao, H, Liu, J & Wang, D 2019, 'Simultaneous energy transfer from molecular-like silver nanoclusters to Sm³⁺/Ln³⁺ (Ln = Eu or Tb) in glass under UV excitation', *Opt. Express*, vol. 27, pp. 38159-38167, <https://doi.org/10.1364/OE.380860>

Thai, NL, Bui, TM, Le, AT & Thi, DAN 2023, 'Utilization of BaAl_{1.4}Si_{0.6}O_{3.4}N_{0.6}:Eu²⁺ green-emitting phosphor to improve luminous intensity and color adequacy of white light-emitting diodes', *International Journal of Technology*, vol. 14, no. 1, pp. 119-128, <https://doi.org/10.14716/ijtech.v14i1.5666>

Thi, MHN, Thai, NL, Bui, TM & Ho, SD 2023, 'The light features and bredigite layout for orthosilicate phosphor in WLED devices', *International Journal of Technology*, vol. 14, no. 4, pp. 911-920, <https://doi.org/10.14716/ijtech.v14i4.5785>

Thi, MHN, Thai, NL, Bui, TM & Thao, NTP 2023, 'Ca₈MgY(PO₄)₇:Eu²⁺,Mn²⁺: A promising phosphor in near-ultraviolet WLED devices', *International Journal of Technology*, vol. 14, no. 3, pp. 501-509, <https://doi.org/10.14716/ijtech.v14i3.5904>

Toslak, D, Son, T, Erol, MK, Kim, H, Kim, T, Chan, RVP & Yao, X 2020, 'Portable ultra-widefield fundus camera for multispectral imaging of the retina and choroid', *Biomed. Opt. Express*, vol. 11, pp. 6281-6292, <https://doi.org/10.1364/BOE.406299>

Tran, A-MD, Anh, NDQ & Loan, NTP 2020, 'Enhancing light sources color homogeneity in high-power phosphor-based white LED using ZnO particles', *Telkomnika*, vol. 18, p. 2628, <http://doi.org/10.12928/telkomnika.v18i5.14198>

Tran, TC, Anh, NDQ & Loan, NTP 2020, 'Excellent color quality of phosphor converted white light emitting diodes with remote phosphor geometry', *Telkomnika*, vol. 18, p. 2757, <http://doi.org/10.12928/telkomnika.v18i5.13575>

Tung, HT, Loan, NTP & Anh, NDQ, 2024, 'The enhancement chromatic uniformity and light-emitting Flux of WLEDs with dual-layer phosphorus configuration', *Lecture notes in electrical engineering*, 2024, pp. 167–174, http://doi.org/10.1007/978-981-99-8703-0_14

Tung, HT, Minh, BT, Thai, NL, Lee, HY & Anh, NDQ 2024, 'ZNO particles as scattering centers to optimize color production and lumen efficiencies of warm white LEDs', *Optoelectronics and Advanced Materials - Rapid Communications*, vol. 18, pp. 1–6

Tung, HT, Thi, MHN & Anh, NDQ 2024, 'Improved color uniformity in white light-emitting diodes using LILU(MOO₄)₂:SM³⁺ combined SiO₂ composite', *International Journal of Technology*, vol. 15, p. 8, <https://doi.org/10.14716/ijtech.v15i1.6165>

Wang, G & Sun, S 2020, 'Fabrication of a mesoporous silica film based optical waveguide sensor for detection of small molecules', *Applied Optics*, vol. 59, no. 13, pp. 3933-3941, <https://doi.org/10.1364/AO.389118>

Wang, Z, Lou, S, Li, P & Lian, Z 2017, 'Single-phase tunable white-light-emitting Sr₃ La(PO₄)₃: Eu²⁺, Mn²⁺ phosphor for white LEDs', *Applied Optics*, vol. 56, no. 4, pp. 1167-1172, <https://doi.org/10.1364/AO.56.001167>

Yang, X, Chai, C, Chen, J, Zheng, S & Chen, C 2019, 'Single 395 nm excitation warm WLED with a luminous efficiency of 104.86 lm/W and a color rendering index of 90.7', *Opt. Mater. Express*, vol. 9, pp. 4273-4286, <https://doi.org/10.1364/OME.9.004273>

Yu, B, Lu, Z, Liang, G, Yuan, Y, Wang, H, He, J & Yang, S 2021, 'Luminous efficacy enhancement for LED lamps using highly reflective quantum dot-based photoluminescent films', *Opt. Express*, vol. 29, pp. 29007-29020, <https://doi.org/10.1364/OE.431345>

Zhang, L, Wang, C, Jin, Y & Xu, T 2022, 'Wide color gamut white light-emitting diodes based on two-dimensional semiconductor nanoplatelets', *Opt. Express*, 30, 3719-3728, <https://doi.org/10.1364/OE.444858>

Zhou, H, Fu, R, Yang, C, Ou, M & Xue, C 2021, 'Influence of calcination temperature on the fluorescence and magnetic properties of Gd₂O₃:Tb³⁺, K⁺ nanoparticles', *Applied Optics*, vol. 60, no. 12, pp. 3302-3307, <https://doi.org/10.1364/AO.418490>